Rapid Communications

Chiral bobbers and skyrmions in epitaxial FeGe/Si(111) films

Adam S. Ahmed,[1] James Rowland,[1] Bryan D. Esser,[2,3] Sarah R. Dunsiger,[4,5]
David W. McComb,[2,3] Mohit Randeria,[1,*] and Roland K. Kawakami[1,†]
[1]*Department of Physics, The Ohio State University, Columbus, Ohio 43210, USA*
[2]*Center for Electron Microscopy and Analysis, The Ohio State University, Columbus, Ohio 43210, USA*
[3]*Department of Materials Science and Engineering, The Ohio State University, Columbus, Ohio 43210, USA*
[4]*Center for Emergent Materials, The Ohio State University, Columbus, Ohio 43210, USA*
[5]*Department of Physics, Simon Fraser University, Burnaby, British Columbia, Canada V5A 1S6*

(Received 26 June 2017; published 17 April 2018)

We report experimental and theoretical evidence for the formation of chiral bobbers—an interfacial topological spin texture—in FeGe films grown by molecular beam epitaxy. After establishing the presence of skyrmions in FeGe/Si(111) thin-film samples through Lorentz transmission electron microscopy and the topological Hall effect, we perform magnetization measurements that reveal an inverse relationship between the film thickness and the slope of the susceptibility ($d\chi/dH$). We present evidence for the evolution as a function of film thickness L from a skyrmion phase for $L < L_D/2$ to a cone phase with chiral bobbers at the interface for $L > L_D/2$, where $L_D \sim 70$ nm is the FeGe pitch length. We show using micromagnetic simulations that chiral bobbers, earlier predicted to be metastable, are in fact the stable ground state in the presence of an additional interfacial Rashba Dzyaloshinskii-Moriya interaction.

DOI: 10.1103/PhysRevMaterials.2.041401

Skyrmions are localized spin textures that exist in magnetic materials where spatial inversion symmetry is broken [1–8]. In such systems, the Dzyaloshinskii-Moriya interaction (DMI) favoring perpendicular alignment of neighboring spins competes with the ferromagnetic exchange interaction and magnetic anisotropy to form a variety of noncollinear and noncoplanar spin textures including skyrmion, helical, and conical phases, whose stability depends on the external magnetic field (H) and temperature (T). The most well studied are the noncentrosymmetric $B20$ crystals such as MnSi [5,9] and FeGe [10], where the phase is restricted to a small pocket of the bulk H-T phase diagram near the magnetic ordering transition. Interestingly, studies of FeGe thin films produced either by thinning bulk crystals or by epitaxial growth have shown that the skyrmion phase occupies a much larger region of the H-T phase diagram [10–12]. This enhanced stability of skyrmions has motivated theoretical studies of magnetic phase diagrams and novel spin textures in thin films [13–18].

One of the fascinating predictions for thin films of noncentrosymmetric materials is the presence of new spin textures forming at the surfaces and interfaces, including the "chiral bobber" [19] and "stacked spiral" [20] phases. In Fig. 1, we illustrate the interfacial chiral bobber crystal [Fig. 1(a)] and compare with the well-known bulk skyrmion crystal [Fig. 1(b)]. The skyrmion phase consists of a hexagonal array of skyrmion tubes that extend throughout the crystal and are aligned with the external magnetic field. Each skyrmion tube consists of magnetic moments that wind about its centerline with a topological charge of one. Like skyrmions, chiral bobbers [Fig. 1(a)] have moments that wind around a centerline and carry topological charge. However, unlike skyrmions, chiral bobbers are localized to the surface of a film in a region with thickness $\sim L_D/2$, where L_D is the helical pitch length, and terminate at a singular point (Bloch point). The remainder of the films is the topologically trivial cone phase. Until now, it has been unclear whether the chiral bobber phase could be realized because previous calculations [19] could only establish that it is a metastable state, not a true ground state.

In this Rapid Communication, we report experimental and theoretical evidence for a stable chiral bobber region through magnetization measurements on a series of epitaxial FeGe thin films grown by molecular beam epitaxy (MBE). After establishing the presence of skyrmions in our FeGe/Si(111) samples with thickness $< L_D$ through Lorentz transmission electron microscopy (LTEM) and the topological Hall effect, we investigate the magnetic phase diagram through magnetization measurements (M vs H) and analysis of the susceptibility curves (χ vs H) for different temperatures and film thicknesses (L). We provide evidence for interfacial chiral bobbers using a combination of experiment and theory. We show that the experimentally measured susceptibility has a slope ($d\chi/dH$) that is constant for $L < L_D/2$, and scales as $1/L$ for $L > L_D/2$. This implies an interfacial spin texture which penetrates a distance $L_D/2$ into the sample. We then use micromagnetic calculations to identify this spin texture as a skyrmion lattice in the very thin films and a chiral bobber lattice on the surface of a bulk cone phase in the thicker samples. We need to include two different ingredients—interface DMI and magnetic anisotropy—in the simulations to understand the experimental observations. It is known that the bulk (Dresselhaus) DMI of $B20$ materials leads only to metastable [19] chiral bobbers in the thin-film geometry. We show that interface (Rashba) DMI, arising from

*randeria.1@osu.edu
†kawakami.15@osu.edu

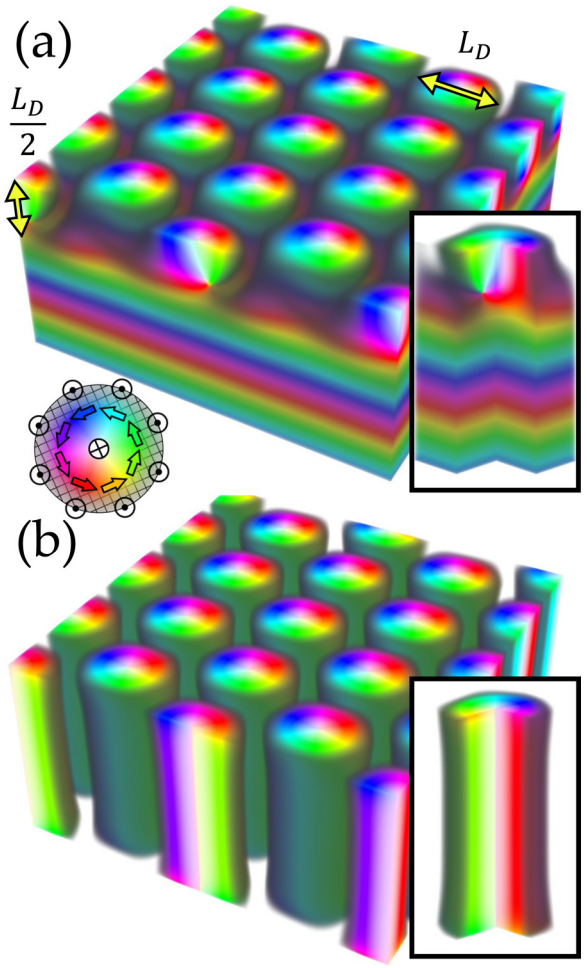

FIG. 1. Examples of two different topological spin textures. (a) Chiral bobber crystal confined to the surface where the bulk is the conical phase. Inset: A 3/4 turn of a chiral bobber shown above the cone phase. (b) Skyrmion crystal. Inset: A 3/4 turn of a single skyrmion tube shown to extend through the entire sample. The color wheel indicates the orientation of the in-plane spins that turn in a counterclockwise fashion. The center point (white) indicates a spin into the page, and the gray/transparent perimeter are spins pointing out of the page.

broken surface inversion symmetry [13,18] in a thin film, together with the bulk DMI, leads to stable interfacial chiral bobbers. Further, an analysis of our experimental saturation fields indicates an effective easy-plane magnetic anisotropy (K_{eff}) in our films. We show that this too is an important input parameter in the micromagnetic simulations that give us insight into the evolution from skyrmions to chiral bobbers with increasing film thickness.

Experiments are performed on FeGe/Si(111) films grown using MBE [21] and characterized using x-ray diffraction, atomic force microscopy, and cross-sectional TEM. Details of growth and characterization are found in the Supplemental Material [22] (which includes Refs. [23–26]).

We perform LTEM measurements to demonstrate the presence of skyrmions in our FeGe films and establish the high quality of our material, and measure the topological Hall effect to show consistency with previous experiments on sputtered

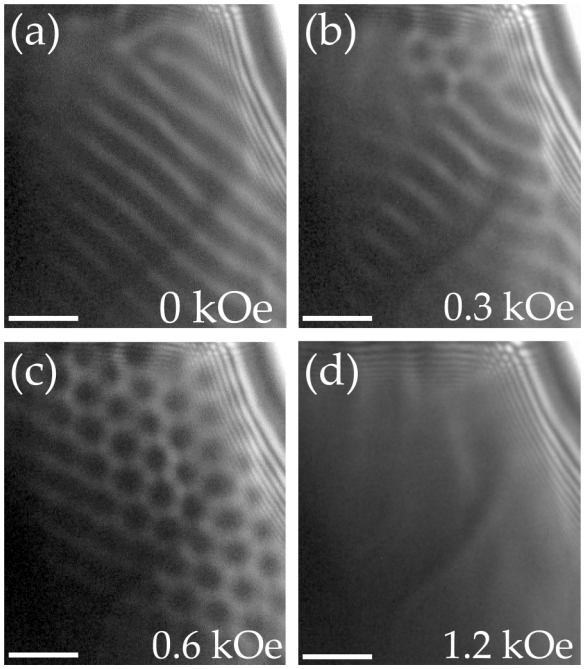

FIG. 2. Series of LTEM images on a 55-nm-thick cross section of an epitaxial FeGe film at 260 K. Both the $[1\bar{1}0]$ crystal axis and the applied magnetic field point into the page. Different magnetic textures are shown for different field values. (a) 0 T: Helical phase. (b) 0.3 kOe: Coexistence of a skyrmion crystal and the helical phase. (c) 0.6 kOe: Only skyrmion crystal present. (d) 1.2 kOe: Field-polarized state. Scale bars are 250 nm.

FeGe films [11,12]. For the LTEM measurements, we extract a ∼55-nm-thick cross section from an epitaxial 1-μm-thick FeGe/Si(111) film, which takes advantage of standard TEM sample processing with focused ion beam milling. Figure 2 shows four representative LTEM images measured at $T = 260\,\text{K}$ with different magnetic fields H applied along the transmission direction. For zero field [Fig. 2(a)], the stripe pattern indicates the presence of the helical phase. For 0.3 kOe [Fig. 2(b)], we observe the coexistence of the skyrmion phase (hexagonal lattice) and the helical phase (stripes). At 0.6 kOe [Fig. 2(c)], the helical phase has disappeared, giving way to the skyrmion phase. Finally, for 1.2 kOe [Fig. 2(d)], the disappearance of magnetic domain contrast signifies the field-polarized state. These LTEM images establish a qualitative baseline for the evolution of magnetic phases as a function of applied magnetic field along $[1\bar{1}0]$. We note that all other magnetic measurements (including topological Hall) have a different sample geometry with the field along [111].

Next, we measure the topological Hall effect of a 35-nm FeGe film on Si(111), which is commonly used as a measure of the "topological charge" density and can be suggestive of the presence of skyrmions. The topological Hall resistivity ρ_{THE} is determined by etching the film into a Hall bar structure, measuring the Hall resistivity, and subtracting contributions from the ordinary Hall effect and anomalous Hall effects (details of the measurement and data analysis are provided in the Supplemental Material [22]). Figure 3(a) shows ρ_{THE} as a function of applied field measured at $T = 50\,\text{K}$. We observe a hysteresis by comparing the upsweep and downsweep, with

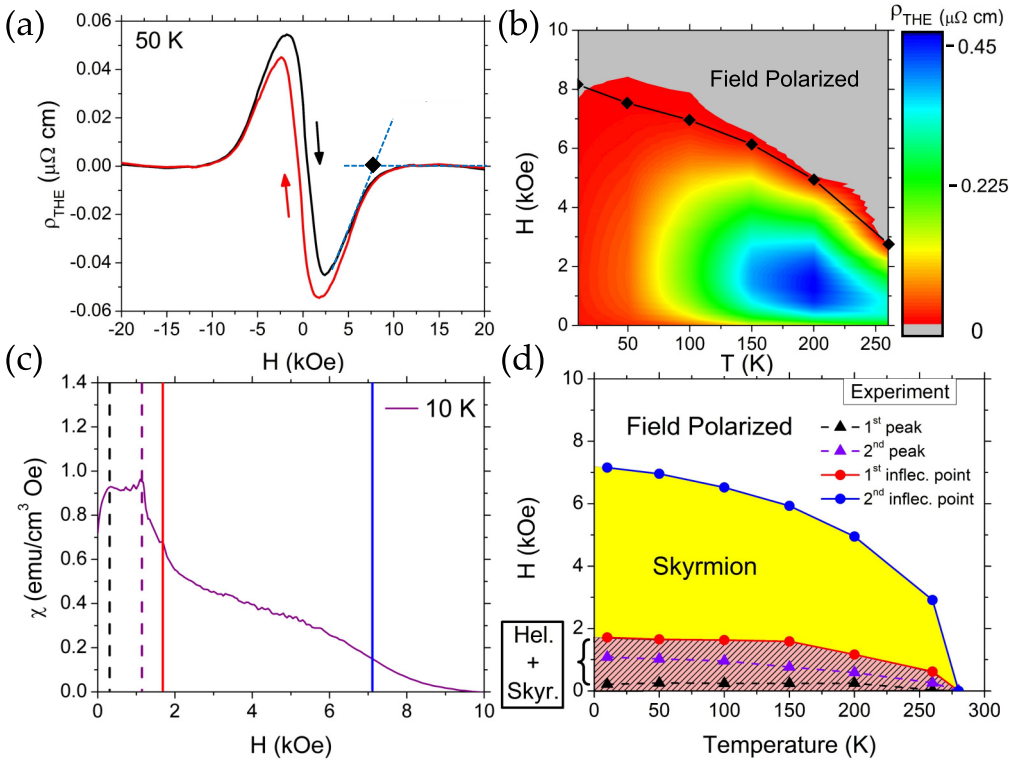

FIG. 3. Electrical and magnetic properties of a 35-nm epitaxial FeGe/Si(111) film. (a) Topological Hall resistivity vs applied magnetic field at 50 K is hysteretic in applied field: Up scan (black curve) and down scan (red curve). The black diamond represents the zero crossing at high fields. The data were antisymmetrized (see Supplemental Material [22]). (b) Average topological Hall resistivity as a function of field and temperature (10, 50, 100, 150, 200, and 260 K). The black line (comprising the extrapolated THE zero crossings) represents the boundary between region of topological density and the field-polarized regime. (c) Susceptibility obtained by numerical differentiation of M vs H curves. SQUID scans are performed after cooling in zero field and measuring with increasing field steps. Solid lines indicate inflection points and dashed lines indicate peaks. (d) Magnetic phase diagram determined by features in the susceptibility data.

a remanence of 42% at zero field. To obtain a H-T mapping of ρ_{THE}, we measure the ρ_{THE} vs H for a series of temperatures and plot ρ_{THE} in the color plot of Fig. 3(b). In contrast to phase diagrams for bulk FeGe with small regions of skyrmion stability [27,28], the topological Hall effect occupies a wider range of the H-T diagram. Notably, the observation of hysteresis and expanded H-T range for ρ_{THE} in our MBE-grown films is consistent with previous studies of ρ_{THE} in sputter-deposited FeGe films [11,12].

To search for different magnetic phases in the FeGe films, we follow the methodology established by Bauer *et al.* [29,30] and perform magnetization measurements as a function of magnetic field, temperature, and film thickness. For all FeGe/Si(111) thin films, we employ a zero-field-cooled protocol to the desired temperature and measure M vs H ramping from $H = 0$ to 20000 Oe in a superconducting quantum interference device (SQUID) magnetometer. Next, taking the numerical derivative yields the susceptibility $\chi = dM/dH$ vs H. Figure 3(c) shows χ vs H for a 35-nm FeGe film. The inflection points of χ correspond to phase transitions into different magnetic states (indicated by solid lines), local maxima correspond to magnetic structures in a state of coexistence (indicated by dashed lines) [23], and the low-field double-peak structure is believed to be related to helical reorientation in our films [31] (see the discussion in the Supplemental Material [22]). We repeat this procedure for a series of temperatures and generate the H-T magnetic phase diagram shown in Fig. 3(d), where the solid lines represent the phase boundaries and the dashed lines are the local maxima of χ. Based on the magnetic phases observed in LTEM (Fig. 2) and the H-T diagram for the topological Hall effect [Fig. 3(b)], we assign the three phases as "helical+skyrmion" for low fields, "skyrmion" for intermediate fields, and "field polarized" for high fields.

Exploring the thickness dependence of χ vs H identifies exciting behavior. Figures 4(a)–4(c) show χ vs H for 35-, 80-, and 500-nm FeGe films, respectively. Looking at the 500-nm film in Fig. 4(c), there is a clear region of constant χ as a function of field. The blue region between 2.5 and 5.0 kOe represents the magnetic phase in this intermediate-field range away from phase boundaries. We continue to track the evolution of this magnetic phase in this field range down to our thinnest samples. Comparing the three thicknesses in this field range, there is clearly a change in the slope of susceptibility $d\chi/dH$. Figure 4(d) shows the χ vs H data in this field range for film thicknesses ranging from 14 to 1000 nm where the slope of χ clearly shows a thickness dependence. To understand the sign and thickness dependence of $d\chi/dH$, let us first focus on the thinnest films with L much less than $L_{\mathrm{D}} \sim 70$ nm [10,32,33]. The measured susceptibility is clearly decreasing as a function of H in the same field regime

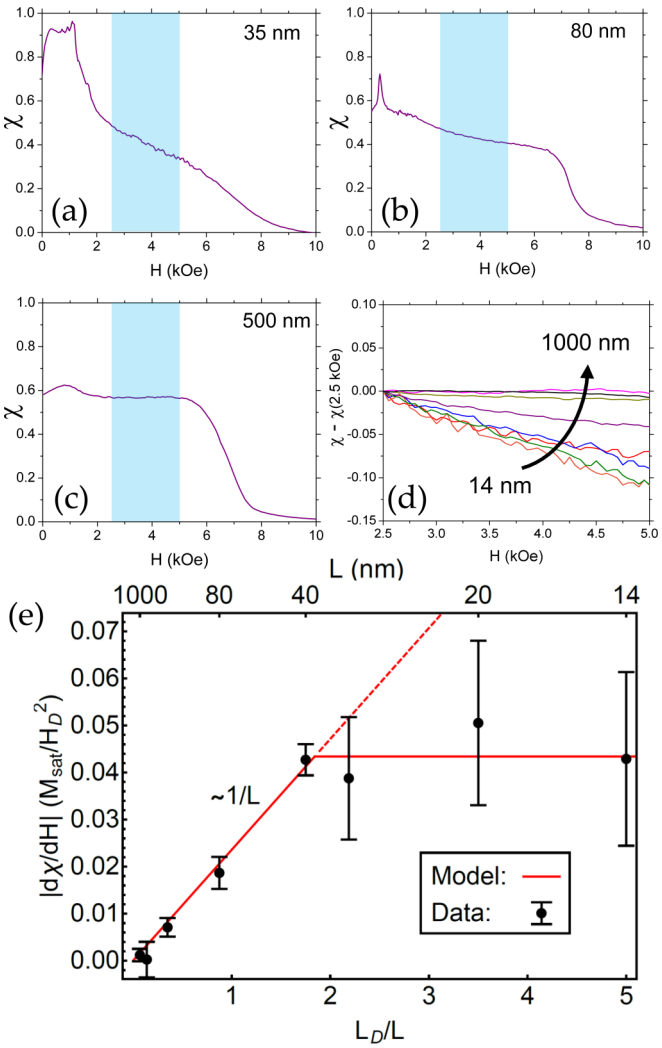

FIG. 4. (a)–(c) Susceptibility vs magnetic field measured at 10 K for 35-, 80-, and 500-nm thickness of FeGe, respectively. The field is applied along the surface normal (growth direction). (d) Susceptibility χ-χ (2.5 kOe) vs magnetic field taken at 10 K and plotted between 2.5 and 5 kOe for film thicknesses from 14 to 1000 nm. (e) Magnitude of $d\chi/dH$ plotted vs inverse thickness L_D/L, with $L_D = 70$ nm. For thicknesses greater than 40 nm, $d\chi/dH$ follows a $1/L$ trend indicative of a surface phenomenon. For thicknesses less than 40 nm, $d\chi/dH$ deviates from the $1/L$ line (dashed red line) and is constant. Note: M_{sat} is the saturation magnetization, and H_D is the saturation field.

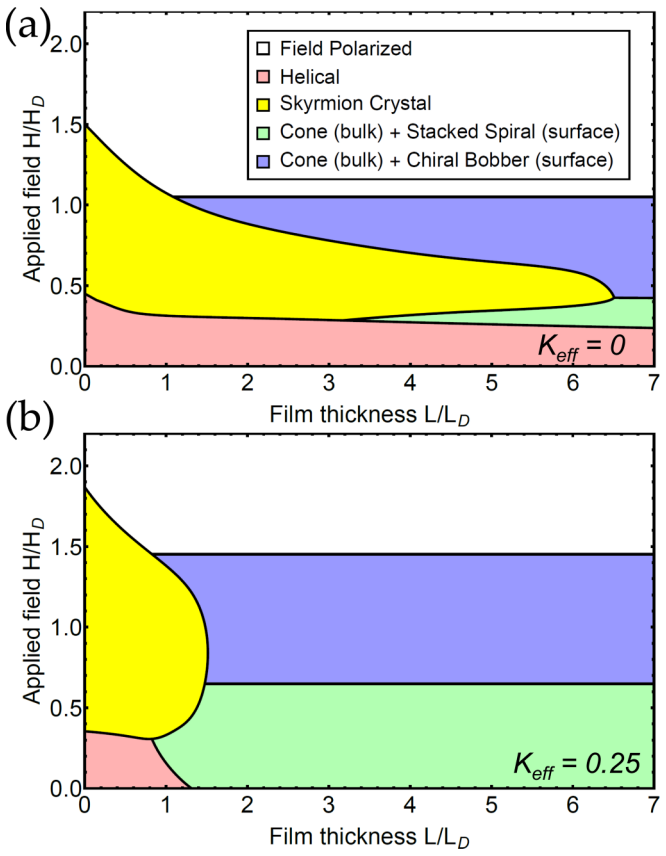

FIG. 5. Applied field vs film thickness phase diagrams at $T = 0$ K calculated from micromagnetics. (a) Phase diagram with bulk and interface DMI and $K_{eff} = 0$ (no anisotropy). With sufficient interface DMI, the chiral bobber/cone phase becomes the true ground state instead of the pure cone phase. For $L/L_D \sim 1-6$, the chiral bobber/cone phase and the skyrmion phase have large regions of stability. (b) Phase diagram with bulk and interface DMI and $K_{eff} = 0.25$ (easy-plane anisotropy). The skyrmion phase is confined to low thicknesses, and the chiral bobber/cone phase dominates for $L/L_D \sim 1-6$. In addition, the stacked spiral/cone phase replaces the helical phase at low fields.

where our micromagnetic simulations indicate a skyrmion state, and we observe a topological Hall effect indicative of topological spin textures (see, e.g., Fig. 3). Microscopically, our micromagnetic simulations show that negative sloped susceptibility is related to the reduction of the skyrmion core and chiral bobber core radius with increasing magnetic field (see the Supplemental Material [22]) which is substantiated by electron holography on thinned FeGe samples [34]. We thus use negative $d\chi/dH$ in the 35-nm film as indicative of a skyrmion state that evolves into a different spin texture with increasing thickness.

From Fig. 4(e) we see that there are two distinct regimes in the plot of the magnitude of the slope of the susceptibility $|d\chi/dH|$ as a function of $1/L$. For small thicknesses ($L < L_D/2$), we find that $|d\chi/dH|$ is independent of film thickness L, while for thicker films ($L > L_D/2$) the slope magnitude scales as $1/L$. We next argue that such a scaling with L, with a crossover at $L_D/2$, is an unambiguous signature for an interface topological spin texture.

The illustration in Fig. 1(a) depicts a film in the large L regime, with chiral bobbers at the top interface. In this regime, the chiral bobber occupies a fixed volume (area $\times L_D/2$) while the cone phase occupies the remainder of the sample of thickness L. As seen from Fig. 1(a), the chiral bobber is akin to a skyrmion at the surface, but which pinches off at a "Bloch point" at a depth $L_D/2$ from the interface, as it merges with the conical texture in the interior. We note that the conical phase has a field-independent χ, so it makes no contribution to $d\chi/dH$. Because χ is an intensive quantity (i.e., per unit volume), the contribution of chiral bobbers would scale as $\sim 1/L$, as seen in Fig. 4(e). On the other hand, for a small thickness ($L < L_D/2$), the film can be thought of as "all interface" and there is no distinction between the chiral bobber and the skyrmion tube because both penetrate through the entire film. In this case, the

contribution of the topological spin texture to χ is independent of film thickness. We note that another interfacial spin texture called a stacked spiral [20] can also be stable in chiral magnetic systems, but we can rule out the possibility of stacked spirals forming in the region of negative $d\chi/dH$ as they are stabilized in low fields [see Fig. 5(b)].

A final point to address is whether chiral bobbers can be stabilized. Previous calculations [19] show that with bulk DMI, chiral bobbers exist only as metastable textures on the surface of a cone phase, even in the presence of surface twists [35] that arise from free boundary conditions in thin films. However, an important consequence of the broken surface inversion symmetry in this geometry is the interface (Rashba) DMI. We present in Fig. 5 the phase diagram based on micromagnetic simulations involving an energy functional that includes both interface and bulk DMI, as required by symmetry for a $B20$ thin film on a substrate, in addition to the effects of surface twists [35]. We find that a chiral bobber crystal is now stabilized at the surface with interfacial DMI, while the rest of the system remains in a cone phase [Fig. 1(a)]; see the Supplemental Material for details [22]. This establishes the theoretical basis for thermodynamically stable chiral bobbers.

We see from the zero-anisotropy phase diagram in Fig. 5(a) that a system with thickness between $L/L_D = 1$ and 6 would exhibit a transition from a skyrmion phase to chiral bobbers with increasing field. This is inconsistent with the experimental χ, which shows a constant negative slope over the entire field range. From an analysis of our magnetization measurements, we find that our films have an effective *easy-plane* anisotropy (see the Supplemental Material [22]). Upon including the effects of easy-plane anisotropy in our simulations, we find [Fig. 5(b)] that skyrmions are stable only for very thin films, while chiral bobbers are seen for large L, consistent with the experimental observations. We also see from Fig. 5(b) that the thick films that harbor chiral bobbers have upper and lower phase boundaries at $0.6H_D = 2.2$ kOe and $1.5H_D = 5.5$ kOe, respectively (using the measured $H_D = M_s D^2/J = 3.7$ kOe), consistent with our observations.

In conclusion, we have synthesized epitaxial FeGe thin films by MBE and investigated their magnetic phase diagram through LTEM, the topological Hall effect, and magnetization measurements. Through systematic measurements of the thickness dependence of susceptibility, we observe a different interface-stabilized spin texture in thin films of noncentrosymmetric skyrmion materials. Micromagnetic simulations show that the presence of the chiral bobber phase stabilized by interface DMI and easy-plane magnetic anisotropy explains both the thickness dependence as well as the magnetic phase diagram observed experimentally. To summarize, our combination of experiment and theory provides compelling evidence for the formation of chiral bobbers in FeGe thin films: The experimental data clearly show the presence of an interfacial magnetic phase and the theoretical analysis identifies it as chiral bobber (+cone phase bulk) with calculated phase boundaries (2.2 and 5.5 kOe) that are consistent with the experimental field range. These results highlight the considerable potential for generating different magnetic phases in thin films and multilayers of $B20$ materials [21].

Note added. Recently, we became aware of another study [36] which detected metastable chiral bobbers with a different experimental technique.

A.S.A. and R.K.K. acknowledge support from the Ohio State Materials Seed Grant (MTB-G00010). B.D.E. and D.W.M. acknowledge support from the Center for Emergent Materials at the Ohio State University, a National Science Foundation Materials Research Science and Engineering Center (Grant No. DMR-1420451), as well as the Ohio State Materials Seed Grant (MTB-G00012), and partial support from the Center for Electron Microscopy and Analysis. M.R. acknowledges support from NSF DMR-1410364. J.R. acknowledges support from the NSF graduate fellowship. S.R.D. acknowledges support from the NSF MRSEC (Grant No. DMR-1420451). The Ohio State University Materials Research Seed Grant Program is funded by the Center for Emergent Materials, an NSF-MRSEC (DMR-1420451), the Center for Exploration of Novel Complex Materials (ENCOMM), and the Institute for Materials Research. We also acknowledge support from the Defense Advanced Research Projects Agency (Grant No. D18AP00008).

[1] N. Kanazawa, S. Seki, and Y. Tokura, Adv. Mater. **29**, 1603227 (2017).
[2] N. Nagaosa and Y. Tokura, Nat. Nanotechnol. **8**, 899 (2013).
[3] W. Jiang, P. Upadhyaya, W. Zhang, G. Yu, M. B. Jungfleisch, F. Y. Fradin, J. E. Pearson, Y. Tserkovnyak, K. L. Wang, O. Heinonen, S. G. E. te Velthuis, and A. Hoffmann, Science **349**, 283 (2015).
[4] K. Litzius, I. Lemesh, B. Kruger, P. Bassirian, L. Caretta, K. Richter, F. Buttner, K. Sato, O. A. Tretiakov, J. Forster, R. M. Reeve, M. Weigand, I. Bykova, H. Stoll, G. Schutz, G. S. D. Beach, and M. Klaui, Nat. Phys. **13**, 170 (2016).
[5] A. Neubauer, C. Pfleiderer, B. Binz, A. Rosch, R. Ritz, P. G. Niklowitz, and P. Böni, Phys. Rev. Lett. **102**, 186602 (2009).
[6] P. Milde, D. Köhler, J. Seidel, L. M. Eng, A. Bauer, A. Chacon, J. Kindervater, S. Mühlbauer, C. Pfleiderer, S. Buhrandt, C. Schütte, and A. Rosch, Science **340**, 1076 (2013).
[7] N. Romming, C. Hanneken, M. Menzel, J. E. Bickel, B. Wolter, K. von Bergmann, A. Kubetzka, and R. Wiesendanger, Science **341**, 636 (2013).
[8] U. K. Rößler, A. N. Bogdanov, and C. Pfleiderer, Nature (London) **442**, 797 (2006).
[9] M. Janoschek, F. Jonietz, P. Link, C. Pfleiderer, and P. Böni, J. Phys.: Conf. Ser. **200**, 032026 (2010).
[10] X. Z. Yu, N. Kanazawa, Y. Onose, K. Kimoto, W. Z. Zhang, S. Ishiwata, Y. Matsui, and Y. Tokura, Nat. Mater. **10**, 106 (2011).
[11] S. X. Huang and C. L. Chien, Phys. Rev. Lett. **108**, 267201 (2012).

[12] J. C. Gallagher, K. Y. Meng, J. T. Brangham, H. L. Wang, B. D. Esser, D. W. McComb, and F. Y. Yang, Phys. Rev. Lett. **118**, 027201 (2017).
[13] J. Rowland, S. Banerjee, and M. Randeria, Phys. Rev. B **93**, 020404 (2016).
[14] S.-Z. Lin, C. Reichhardt, C. D. Batista, and A. Saxena, Phys. Rev. Lett. **110**, 207202 (2013).
[15] S.-Z. Lin, A. Saxena, and C. D. Batista, Phys. Rev. B **91**, 224407 (2015).
[16] X. Li, W. V. Liu, and L. Balents, Phys. Rev. Lett. **112**, 067202 (2014).
[17] M. N. Wilson, A. B. Butenko, A. N. Bogdanov, and T. L. Monchesky, Phys. Rev. B **89**, 094411 (2014).
[18] S. Banerjee, J. Rowland, O. Erten, and M. Randeria, Phys. Rev. X **4**, 031045 (2014).
[19] F. N. Rybakov, A. B. Borisov, S. Blügel, and N. S. Kiselev, Phys. Rev. Lett. **115**, 117201 (2015).
[20] F. N. Rybakov, A. B. Borisov, S. Blügel, and N. S. Kiselev, New J. Phys. **18**, 45002 (2016).
[21] A. S. Ahmed, B. D. Esser, J. Rowland, D. W. McComb, and R. K. Kawakami, J. Cryst. Growth **467**, 38 (2017).
[22] See Supplemental Material at http://link.aps.org/supplemental/10.1103/PhysRevMaterials.2.041401 for details of growth, topological Hall measurements and extraction, magnetization measurements, micromagnetic simulations, and a discussion about negative sloped susceptibility, which includes Refs. [23–26].
[23] I. Levatić, V. Šurija, H. Berger, and I. Živković, Phys. Rev. B **90**, 224412 (2014).
[24] A. Vansteenkiste, J. Leliaert, M. Dvornik, M. Helsen, F. Garcia-Sanchez, and B. Van Waeyenberge, AIP Adv. **4**, 107133 (2014).
[25] T. Adams, A. Chacon, M. Wagner, A. Bauer, G. Brandl, B. Pedersen, H. Berger, P. Lemmens, and C. Pfleiderer, Phys. Rev. Lett. **108**, 237204 (2012).
[26] M. Beg, R. Carey, W. Wang, D. Cortés-Ortuño, M. Vousden, M.-A. Bisotti, M. Albert, D. Chernyshenko, O. Hovorka, R. L. Stamps, and H. Fangohr, Sci. Rep. **5**, 17137 (2015).
[27] H. Wilhelm, M. Baenitz, M. Schmidt, C. Naylor, R. Lortz, U. K. Rößler, A. A. Leonov, and A. N. Bogdanov, J. Phys.: Condens. Matter **24**, 294204 (2012).
[28] H. Wilhelm, M. Baenitz, M. Schmidt, U. K. Rößler, A. A. Leonov, and A. N. Bogdanov, Phys. Rev. Lett. **107**, 127203 (2011).
[29] A. Bauer and C. Pfleiderer, Phys. Rev. B **85**, 214418 (2012).
[30] A. Bauer and C. Pfleiderer, in *Topological Structures in Ferroic Materials*, edited by J. Seidel, Springer Series in Mater. Sci. (Springer, Cham, 2016), Vol. 228, p. 1.
[31] A. Bauer, A. Chacon, M. Wagner, M. Halder, R. Georgii, A. Rosch, C. Pfleiderer, and M. Garst, Phys. Rev. B **95**, 024429 (2017).
[32] N. A. Porter, C. S. Spencer, R. C. Temple, C. J. Kinane, T. R. Charlton, S. Langridge, and C. H. Marrows, Phys. Rev. B **92**, 144402 (2015).
[33] B. Lebech, J. Bernhard, and T. Freltoft, J. Phys.: Condens. Matter **1**, 6105 (1989).
[34] K. Shibata, A. Kovács, N. S. Kiselev, N. Kanazawa, R. E. Dunin-Borkowski, and Y. Tokura, Phys. Rev. Lett. **118**, 087202 (2017).
[35] A. O. Leonov, Y. Togawa, T. L. Monchesky, A. N. Bogdanov, J. Kishine, Y. Kousaka, M. Miyagawa, T. Koyama, J. Akimitsu, T. Koyama, K. Harada, S. Mori, D. McGrouther, R. Lamb, M. Krajnak, S. McVitie, R. L. Stamps, and K. Inoue, Phys. Rev. Lett. **117**, 087202 (2016).
[36] F. Zheng, F. N. Rybakov, A. B. Borisov, D. Song, S. Wang, Z. Li, H. Du, N. S. Kiselev, J. Caron, A. Kovács, M. Tian, Y. Zhang, S. Blügel, and R. E. Dunin-Borkowski, arXiv:1706.04654.